Magnetism of a single atom

Otte, A.F.

Chapter 3

Magnetic Anisotropy

The work presented in this chapter was published as *Large Magnetic Anisotropy of a Single Atomic Spin Embedded in a Surface Molecular Network*, by C. F. Hirjibehedin, C.-Y. Lin, A. F. Otte, M. Ternes, C. P. Lutz, B. A. Jones, and A. J. Heinrich, Science **317**, 1199 (2007).

3.1 Introduction

Anisotropy is what makes the difference between spin and magnetism. A free atom, regardless of its electronic structure, is always perfectly spherical. Although it may possess a finite amount of spin (as a result of some electron orbitals being half-filled), the lack of anisotropy makes the orientation of the spinning axis intrinsically undetermined and therefore it will never exhibit magnetism. The tendency to align the angular momentum in a certain direction and the ability to maintain the resulting magnetization over an extended amount of time is governed entirely by the atom's immediate environment.

The same is true for large ensembles of spins. Current non-volatile magnetic storage devices (hard drives) are based on a continuous thin film of ferromagnetic material, the magnetic domains of which are much smaller than the bits we intend to write on it. The anisotropy of the material will make sure that each domain has an 'easy-axis' along which it would like to magnetize either up or down. In order to flip a domain one would have to overcome an energy barrier $\Delta\varepsilon = K_u V$ [38]. Here K_u is the anisotropy constant and V the volume of the domain. At a finite temperature T this will happen spontaneously with a rate

$$\frac{1}{\tau} = f_0 \mathrm{e}^{-\Delta\varepsilon/k_B T}, \tag{3.1}$$

where f_0 is a measure of the attempt frequency, typically taken to be 10^9 s^{-1}, and k_B is Boltzmann's constant. A reliable storage medium has $\Delta\varepsilon/k_B T = 50$ or higher. If however from here we reduce the domain volume V by only a factor of 2, the decay time τ will decrease by a factor e^{25} ($\sim 10^{11}$)! Clearly, we are

extremely limited in reducing the domain size and hence the bit size as long as we cannot control the anisotropy. This impending technological barrier, that currently threatens to halt the decades-long trend toward ever higher storage densities at room temperature, is called the *superparamagnetic limit*.

Much larger anisotropies per atom than the ones found in current thin-film magnetic materials have been reported in magnetic structures consisting of only a few atomic spins, such as single atoms and clusters on metal surfaces [39, 40] and molecular magnets [41, 42, 43]. These systems are of technological interest as they have energy barriers that are already high enough to maintain a stable spin orientation at low temperatures.

To lowest order, the energy of a spin in an environment with uniaxial anisotropy (i.e. where only one axis is unique) can be described by [43]:

$$\hat{\mathcal{H}} = -g\mu_B \mathbf{B} \cdot \hat{\mathbf{S}} + D\hat{S}_{\mathcal{Z}}^2. \qquad (3.2)$$

Here the first term is the Zeeman splitting of the states in the presence of a magnetic field, where g is the g-factor, μ_B the Bohr magneton and $\hat{\mathbf{S}} = \left(\hat{S}_{\mathcal{X}}, \hat{S}_{\mathcal{Y}}, \hat{S}_{\mathcal{Z}}\right)$ the spin operator. The anisotropy is represented by the second term which splits the zero-field degeneracy of the spin-states based on the magnitude of the spin's $\mathcal{Z}$-projection m. If $D < 0$, large values of $|m|$ are favored and we can speak of an 'easy-axis'. With $D > 0$, the spin would like to minimize the $\mathcal{Z}$-component of its magnetic moment such that the system has an 'easy-plane' orthogonal to the unique axis. For the first case the effect of this term is sketched in fig. 3.1: a barrier of height $-DS^2$ for integer spin and $-D\left(S^2 - \frac{1}{4}\right)$ for half-integer spin separates the two metastable configurations.

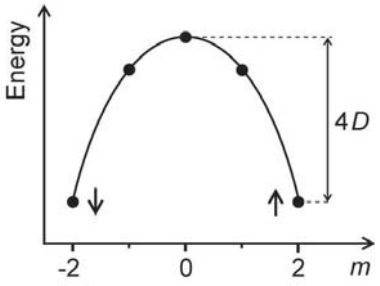

Figure 3.1: Schematic view of the $\hat{S}_{\mathcal{Z}}$ eigenvalues of an $S = 2$ system under axial anisotropy with $D < 0$.

If all three axes are unique we add another term to the Hamiltonian expressing the difference between the remaining two directions (transverse anisotropy):

$$\hat{\mathcal{H}} = -g\mu_B \mathbf{B} \cdot \hat{\mathbf{S}} + D\hat{S}_{\mathcal{Z}}^2 + E\left(\hat{S}_{\mathcal{X}}^2 - \hat{S}_{\mathcal{Y}}^2\right). \qquad (3.3)$$

By convention, the axes are assigned as to maximize $|D|$ and have $E > 0$. Note that we use the coordinate symbols $(\mathcal{X}, \mathcal{Y}, \mathcal{Z})$ to distinguish from the real-world axes (x, y, z), which will be defined in section 3.3. The transverse term does not commute with $\hat{S}_{\mathcal{Z}}$, such that it mixes states with different m. This means that the two magnetization directions no longer represent stationary states as a result of which the system cannot be used as a bit anymore. We can now conclude that an ideal situation for data storage occurs when S is large, D is large and negative and E is very small.

3.2 Cu_2N: a Molecular Network

When an atom is placed upon a surface, obviously the out-of-plane direction becomes unique. In the particular case of atoms bound on the Cu sites of Cu_2N there is a distinction between the two in-plane directions as well: if the atom is positioned on a N-row it is part of a v-column in the other direction or vice versa (a schematic drawing can be found further on in fig. 3.4a). In this section we will look at the exact composition of the Cu_2N surface in more detail.

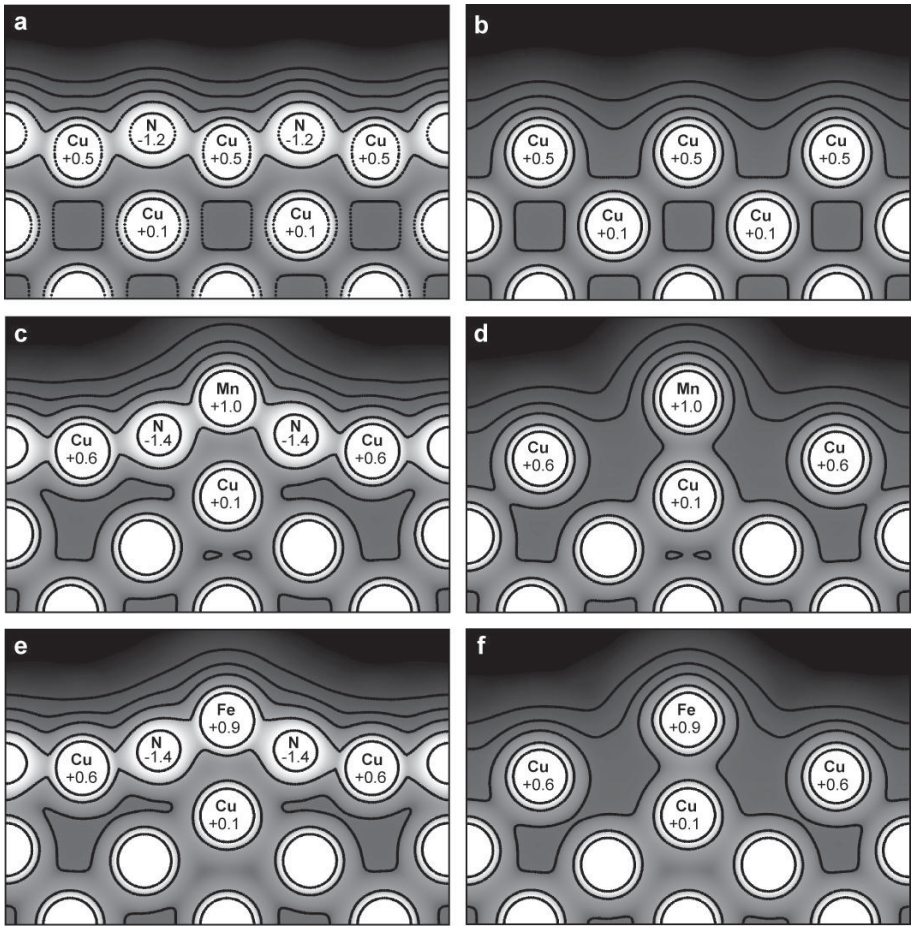

Figure 3.2: DFT calculations of the electron density in the Cu_2N lattice. **(a, b)** Cross-sectional views of bare Cu_2N through a N-row (a) and through a v-row (b). **(c–f)** Same for Cu_2N with a Mn or Fe atom adsorbed onto it. Dark (*light*) regions indicate low (*high*) electron density. The black equal density lines are spaced logarithmically at powers of $10^{1/2}$ e/a_0, where e is the elementary charge and a_0 the Bohr radius. The line at highest density corresponds to $10^{-1/2} \simeq 0.3$ e/a_0. At each atom the net charge is given in units of e.

To better understand the structure formed by magnetic atoms on Cu_2N, we used density functional theory (DFT) calculations of the electron density performed by C.-Y. Lin and B.A. Jones. These were done using the all-electron full-potential linearized augmented plane wave (FLAPW) method [44] with the exchange-correlation potential in the generalized gradient approximation (GGA) [45]. For details of the calculation see [46]. Figures 3.2a and b show cross-sections of the calculated charge density of Cu_2N on Cu(100) in the absence of any adatom, respectively along a N-row and a v-row. The N atoms are seen to be slightly above the plane of the surface Cu atoms. In addition, there is a net transfer of (negative) charge from the Cu atoms to the N atoms. A comparison of the charge densities along the two orientations shows that the Cu_2N has formed a network of polar covalent bonds along the N-rows that is distinct from the underlying bulk copper.

Placing an Mn or Fe atom on top of a Cu atom causes a substantial rearrangement of the atomic structure. As seen in figs. 3.2c–f for both Mn and Fe, the Cu atom directly below the magnetic atom has moved toward the bulk and is no longer part of the polar covalent Cu_2N network. The magnetic atom transfers charge to the Cu_2N surface and creates bonds with its neighboring N atoms: the magnetic atom is thus incorporated into the extended molecular network on the surface. In view of these significant structural and electronic changes involved in placing an atom on the surface, it is all the more surprising that we can reverse the process by removing an adatom as described in the previous chapter without permanently changing the Cu_2N surface.

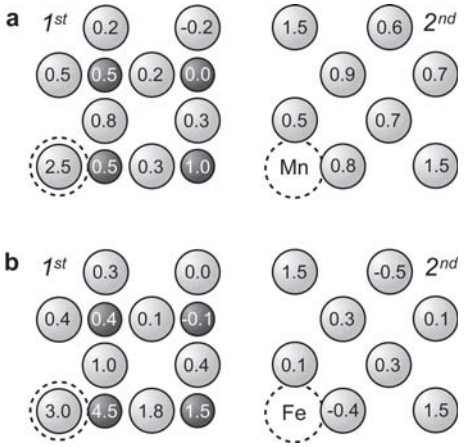

Figure 3.3: Calculations of the local spin density on each atom for **(a)** Mn and **(b)** Fe on Cu_2N. In either case the left (*right*) image shows the first (*second*) layer of atoms. Cu atoms are depicted as large light grey spheres while N atoms are smaller and dark. Dashed circles indicate the position of the adatom above the first layer. The numbers give the net spin ($\times 100$) on each atom and its surrounding interstitial region. Including the spin on the adatoms, these add up to 250 for Mn and 200 for Fe.

The calculations can also give information on the local distribution of spin, determined by evaluating $S = (N_\uparrow - N_\downarrow)/2$ where $N_\uparrow$ and $N_\downarrow$ are the total number of electrons with spin up and down in a specified volume. In the case of Mn, the spin on the atom itself and the surrounding interstitial region is $S = 2.28$, whereas for Fe $S = 1.73$. These values are slightly lower than the free-atom spins (i.e. $S = \frac{5}{2}$ for Mn and $S = 2$ for Fe), however, a substantial amount of spin density extends into the surrounding atoms, as illustrated in fig. 3.3. By including the spin on all of the atoms, the net spin of the total structure is calculated to be the same as that of the free atoms (2.50 and 2.00). Specifically in the case of Fe we find that the spin spreading occurs primarily along the direction of the N-row, while for Mn there seems to be a slightly stronger tendency to spread down into the second layer. This spreading of spin density, here up to 5 Å from the binding site, is similar to that reported in DFT calculations of molecular magnets [48]. In comparison, no substantial net spin density is found for bare Cu_2N on Cu(100).

3.3 Anisotropy in Spin Excitations

The existence of zero-field excitations as seen in the spectra of fig. 2.2, indicating that the different spin orientations (quantum number m) are non-degenerate, suggests that the atomic spins on Cu_2N are subject to strong magneto-crystalline anisotropy. We studied the anisotropy of Mn and Fe atoms on the Cu sites of Cu_2N by following the evolution of their spin excitations when a magnetic field is applied in three orthogonal directions. As discussed in section 1.4 the He dewar in which the 7 T superconducting magnet was mounted could be rotated such that the field was either in the plane of the sample or perpendicular to it. In the second case there was a $\sim 7^\circ$ tilt of the magnetic field with respect to the sample's normal vector which we will ignore during further analysis. When the magnetic field was in the plane, the orientation of the sample was such that the field aligned with the (001)-direction of the crystal, i.e. parallel to the N-rows and v-rows in one direction (in this situation there was a $\sim 5^\circ$ misalignment that we will ignore). Distinction between the two in-plane field directions was made by separately regarding adatoms that were located either on a N-row or on a v-row. As a result, multiple field directions could not be realized on a single atom (without repositioning it). Switching from an in-plane to a perpendicular field even required preparing a whole new sample (section 2.2.1) as it involved dismounting the entire cryostat. For each individual atom lying on a Cu site, we will use the coordinate system as defined for Mn in fig. 3.4a, where x is directed along the N-row, y along the v-row and z is the surface's normal vector.

In the subsequent analysis we will describe each of the atomic spin systems by a single spin vector $\hat{\mathbf{S}}$. It is important to note that this 'spin' is a resultant quantity which comprises both the intrinsic spin of the electrons and their orbital angular momentum. As the crystal field can only directly influence the latter, spin-orbit coupling plays an important role in translating the effects of magnetic anisotropy to the actual electronic spins.

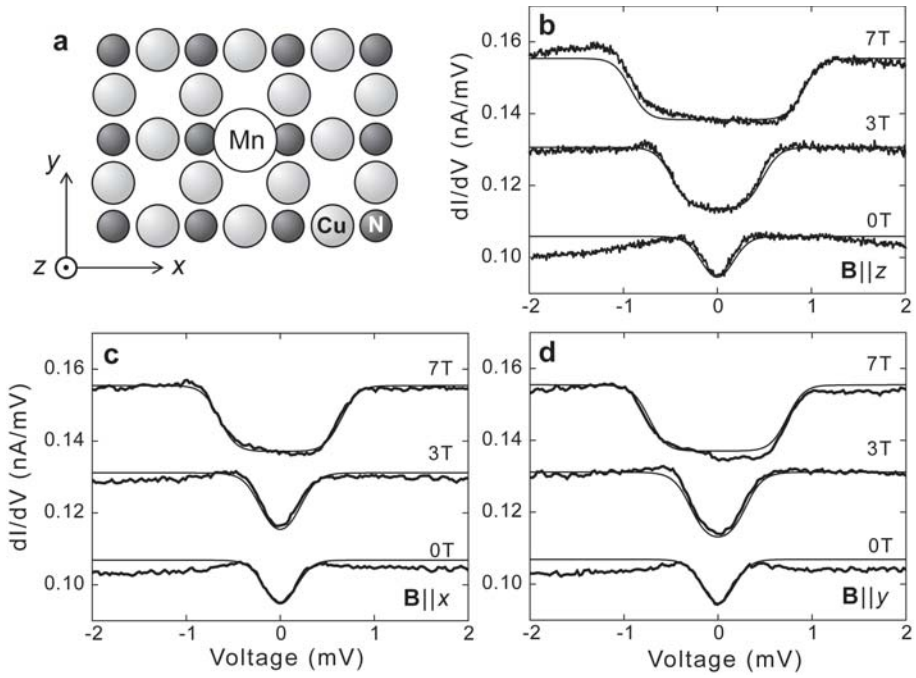

Figure 3.4: (a) Schematic top view of Mn on Cu_2N. This assignment of the axes will be used for any single atom on Cu_2N. **(b–d)** dI/dV-spectra on a individual Mn atoms in various magnetic fields oriented along z, x and y in (b), (c) and (d) respectively. Smooth curves show the calculated conductance based on (3.5), scaled to fit the data.

3.3.1 Mn: a Weak Easy-Axis

Figures 3.4b–d show spin excitation spectra taken on three different Mn atoms, each corresponding to one field direction, at 0 T, 3 T and 7 T. In each situation the energy of the single step that is found symmetrically around zero bias grows with the field strength. The rate at which it grows is nearly equal for $\mathbf{B} \parallel x$ and $\mathbf{B} \parallel y$ (the two in-plane directions), but is markedly higher when $\mathbf{B} \parallel z$. We shall try to explain these observations using the anisotropy Hamiltonian (3.3). Mn is a $3d^5$ metal so we expect its spin to be $\frac{5}{2}$. Since the x and y field orientations give similar results we can expect the main anisotropy axis $\mathcal{Z}$ to coincide with the z-direction, and E to be very small. Fig. 3.5a shows the qualitative effect the anisotropy Hamiltonian has on the energy levels of an $S = \frac{5}{2}$ system when $D < 0$, $E = 0$ and $\mathbf{B} \parallel \mathcal{Z}$. If we assume the transitions to obey the selection rules[1] $\Delta m = 0$ or ± 1, a single transition from the ground state ($m = \frac{5}{2}$) to $m = \frac{3}{2}$ is allowed, the energy of which is finite at $B = 0$ and grows linearly with the field. Note that if we choose $D > 0$, $m = \frac{1}{2}$ would become the ground state and we would have two allowed transitions (to $m = \frac{3}{2}$ and $m = -\frac{1}{2}$).

[1] We will discuss these rules in section 3.3.3.

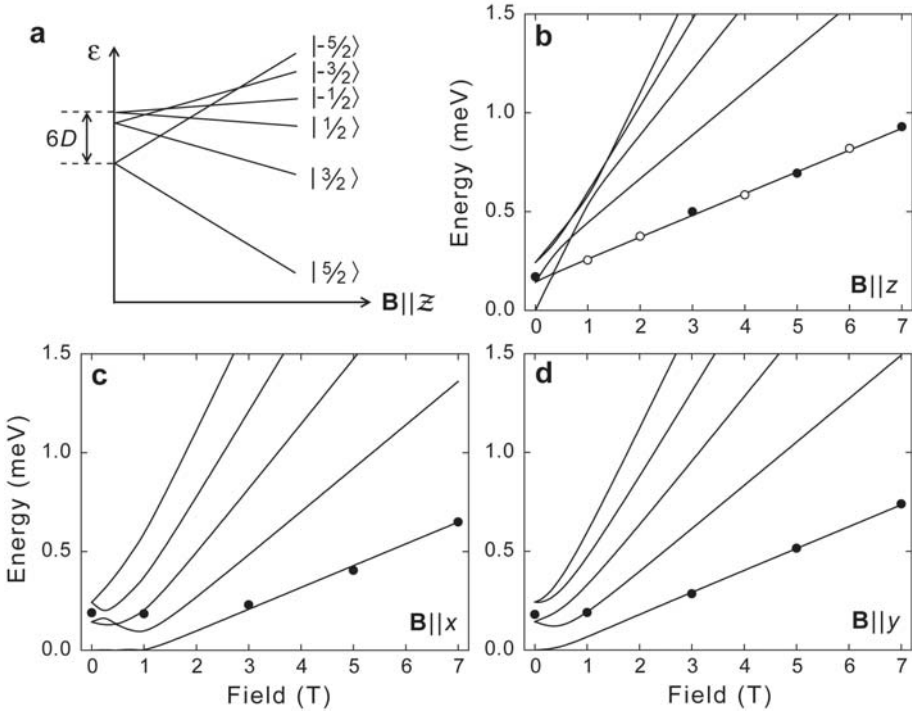

Figure 3.5: **(a)** Sketch of the qualitative effect of a negative D-value on an $S = \frac{5}{2}$ system when the field is oriented along the primary axis $\mathcal{Z}$. **(b–d)** Step energies taken from fig. 3.4. The solid lines indicate excitation energies obtained by diagonalization of 3.3. In (b) the open circles label step energies measured on a different Mn atom.

We obtained the best fit of the step positions when $g = 1.90 \pm 0.01$, $D = -0.039 \pm 0.001$ meV, and $E = 0.007 \pm 0.001$ meV with $(\mathcal{X}, \mathcal{Y}, \mathcal{Z}) = (x, y, z)$. The calculated transition energies for these values are shown in figures 3.5b–d. Due to the weakness of the anisotropy there are many level crossings at low magnetic field. Especially in the x and y-directions, where even at $E = 0$ the levels are not eigenstates of $\hat{S}_z$, this complicates the exact assignment of the spin excitations.

The resulting parameters correspond to a magnetic easy-axis pointing out of the plane (i.e. $\mathcal{Z} = z$). The value of D, which is much smaller than the anisotropy of Fe as will be discussed shortly, is consistent with anisotropy values observed for Mn in molecular magnetic clusters [49]. Small anisotropy is also expected for half filling of the d-orbitals. Hund's rule coupling leads to alignment of the electron spin and single occupation of all d-states, giving rise to a symmetric charge distribution within the d-shell. Although the results indicate a finite value for E, its magnitude is still too small to cause observable transitions to other levels that could arise from mixing of the eigenstates.

3.3.2 Fe: Almost a Bit

The zero-field spectrum of Fe, which based on its electronic configuration ($3d^6$) we expect to behave as an $S = 2$ system[2], features three steps at $|V| \simeq 0.2$, 3.8 and 5.7 mV. These excitation energies change by less than $\sim 5\%$ between various measurements performed on Fe atoms adsorbed on different Cu_2N islands and measured with different tips. This variation may arise from slight changes in the local environment caused by the inherent strain in the Cu_2N islands [50]. The appearance of three spin excitations can be explained by choosing the anisotropy parameters $D < 0$ and $E \neq 0$, as illustrated qualitatively in fig. 3.7a. The result of having a substantial E (and the absence of Kramers degeneracy for integer S, see chapter 4) is that all zero-field degeneracy is broken, including that for equal $|m|$. Now the 0.2 meV step can be assigned to an excitation between $|m| = 2$ states, while the steps at higher energies are signatures of $|m| = 2 \rightarrow 1$ transitions. Excitations to $m = 0$ are forbidden by the selection rules.

The field dependence of the step positions (figs. 3.6a–c) is much more anisotropic than in the case of Mn. A clear example is the 5.7 meV step, that goes up in energy with increasing $\mathbf{B} \parallel x$ and down when $\mathbf{B} \parallel y$. The evolution of the heights of the steps, which is similarly anisotropic, especially for the 0.2 meV excitation, will be discussed in the next section. Calculations of the energy levels, fitting the measured step positions, are plotted in figs. 3.6d–f. The parameters used here are $g = 2.11 \pm 0.05$, $D = -1.55 \pm 0.01$ meV and $E = 0.31 \pm 0.01$ meV, with the anisotropy axes assigned as $(\mathcal{X}, \mathcal{Y}, \mathcal{Z}) = (y, z, x)$. This translates into a strong easy-axis ($\mathcal{Z}$) along the N-direction (x), with a significant contribution from transverse anisotropy. Similar values, although usually with positive D (corresponding to planar or hard-axis anisotropy), have been observed in crystals formed from molecular magnet structures with single Fe atoms [49].

3.3.3 Transition Intensities

In order to better understand the inelastic tunneling process that governs the spin excitations we can additionally analyze the intensity of the observed transitions. We find that the relative step heights in the Fe spectra, which should be a measure of the excitation intensities, are well-described by:

$$\begin{aligned} I_{0\rightarrow n} &= \left|\langle\psi_n|\,\hat{S}_{\mathcal{X}}\,|\psi_0\rangle\right|^2 + \left|\langle\psi_n|\,\hat{S}_{\mathcal{Y}}\,|\psi_0\rangle\right|^2 + \left|\langle\psi_n|\,\hat{S}_{\mathcal{Z}}\,|\psi_0\rangle\right|^2 \\ &= \frac{1}{2}\left\{\left|\langle\psi_n|\,\hat{S}_{+}\,|\psi_0\rangle\right|^2 + \left|\langle\psi_n|\,\hat{S}_{-}\,|\psi_0\rangle\right|^2 + 2\left|\langle\psi_n|\,\hat{S}_{\mathcal{Z}}\,|\psi_0\rangle\right|^2\right\}, \end{aligned} \tag{3.4}$$

where $\hat{S}_{\pm} = \hat{S}_{\mathcal{X}} \pm i\hat{S}_{\mathcal{Y}}$ and the $|\psi_n\rangle$ states are obtained directly from diagonalization of (3.3), with $|\psi_0\rangle$ being the ground state. This expression was also used for analysis of neutron scattering experiments on a similar magnetic system [51]. The first two terms enable $\Delta m = \pm 1$ transitions and the third term

[2] See section 3.4 for a discussion on the validity of using the free-atom value of S.

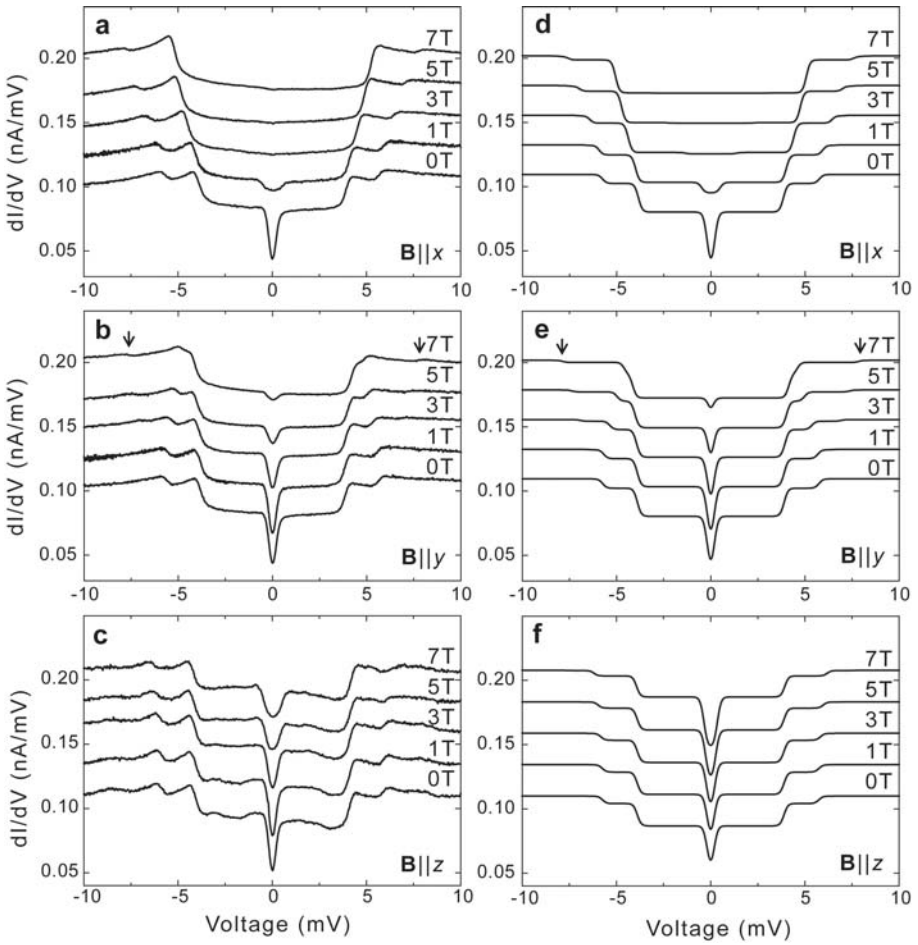

Figure 3.6: Conductance spectra on Fe in various magnetic fields oriented along x **(a)**, y **(b)** and z **(c)**. **(d–f)** Calculated conductance curves based on (3.5). The arrows indicate the appearance of the $|\psi_0\rangle \rightarrow |\psi_4\rangle$ transition.

allows $\Delta m = 0$. These selection rules are consistent with previous empirically observed transitions in STM spin-excitation experiments [19].

Table 3.1 lists the $|\psi_n\rangle$ vectors (still for Fe) in the basis of $\hat{S}_{\mathcal{Z}}$-eigenstates $|m\rangle$. When $B = 0$ T, the ground state $|\psi_0\rangle$ has most weight in the $|{-}2\rangle$ and $|{+}2\rangle$ states. From here, transitions to $|\psi_1\rangle$ ($\Delta m = 0$) and $|\psi_2\rangle$ and $|\psi_3\rangle$ ($\Delta m = \pm 1$) are strong, whereas transitions to $|\psi_4\rangle$ are forbidden. At $B = 7$ T along $\mathcal{Z}$ (i.e. x, the N-row), the situation changes substantially: because most of the weight in $|\psi_0\rangle$ is now in the $|{+}2\rangle$ state, $\Delta m = \pm 1$ transitions to $|\psi_2\rangle$ and $|\psi_3\rangle$ remain visible while transitions to $|\psi_1\rangle$ (now mostly $|{-}2\rangle$) and $|\psi_4\rangle$ are too weak to be observed. This is consistent with the observed disappearance of the 0.2 meV step for $B > 1$ T in the x-direction.

Table 3.1: Eigenvectors for Fe on Cu_2N, written as a sum of $|m\rangle$ states and obtained by diagonalization of (3.3) with $S = 2$, $g = 2.11$, $D = -1.55$ meV and $E = 0.31$ meV, at $B = 0$ T and $B = 7$ T oriented along $\mathcal{Z}$.

Eigenstate	$\|-2\rangle$	$\|-1\rangle$	$\|+0\rangle$	$\|+1\rangle$	$\|+2\rangle$
$B = 0$ T					
$\|\psi_0\rangle$	0.697	0	–0.166	0	0.697
$\|\psi_1\rangle$	0.707	0	0	0	–0.707
$\|\psi_2\rangle$	0	0.707	0	–0.707	0
$\|\psi_3\rangle$	0	0.707	0	0.707	0
$\|\psi_4\rangle$	0.117	0	0.986	0	0.117
$B = 7$ T					
$\|\psi_0\rangle$	0.021	0	–0.097	0	0.995
$\|\psi_1\rangle$	0.987	0	–0.157	0	–0.036
$\|\psi_2\rangle$	0	0.402	0	–0.916	0
$\|\psi_3\rangle$	0	0.916	0	0.402	0
$\|\psi_4\rangle$	0.159	0	0.983	0	0.092

Calculated values for $I_{0\to n}$ with $\mathbf{B} \parallel \mathcal{Z}$ are shown in fig. 3.7b. They are normalized to fit the relative step heights as extracted from the measurements. Note that it would be senseless to compare the absolute step heights. As certain transitions die out the total inelastic current decreases, but each spectrum is started at the same quiescent settings such that other inelastic contributions (i.e. excitation intensities) are rescaled. Therefore we look at the relative composition of the inelastic current, which gives meaningful quantities at any field. A similar calculation with $\mathbf{B} \parallel \mathcal{X}$ (i.e. y, the v-row) indicates that starting from ~ 2 T in this direction the $|\psi_0\rangle \to |\psi_4\rangle$ transition should open up. This may explain the small steps around $|V| = 8$ meV indicated by the arrows in the 7 T spectrum of fig. 3.6b.

We can even model the full conductance spectra as the sum of a voltage-independent elastic conductance and a series of thermally broadened IETS transitions. For the inelastic part of the conductance we use:

$$\begin{aligned}\sigma_{\mathrm{ie}} \quad \propto \quad & \sum_m \sum_{n>m} I_{m\to n} P_m(T)\Big(1 - P_n(T)\Big) \\ & \times \left\{ \Phi\left(\frac{eV + (\varepsilon_n - \varepsilon_m)}{k_B T}\right) + \Phi\left(-\frac{eV - (\varepsilon_n - \varepsilon_m)}{k_B T}\right)\right\}, \end{aligned} \tag{3.5}$$

where each IETS step is weighted by the calculated intensity $I_{m\to n}$ as given by (3.4) and by the Maxwell-Boltzmann distribution:

$$P_i(T) = \frac{\mathrm{e}^{-\varepsilon_i/k_B T}}{\sum_j \mathrm{e}^{-\varepsilon_j/k_B T}} \; . \tag{3.6}$$

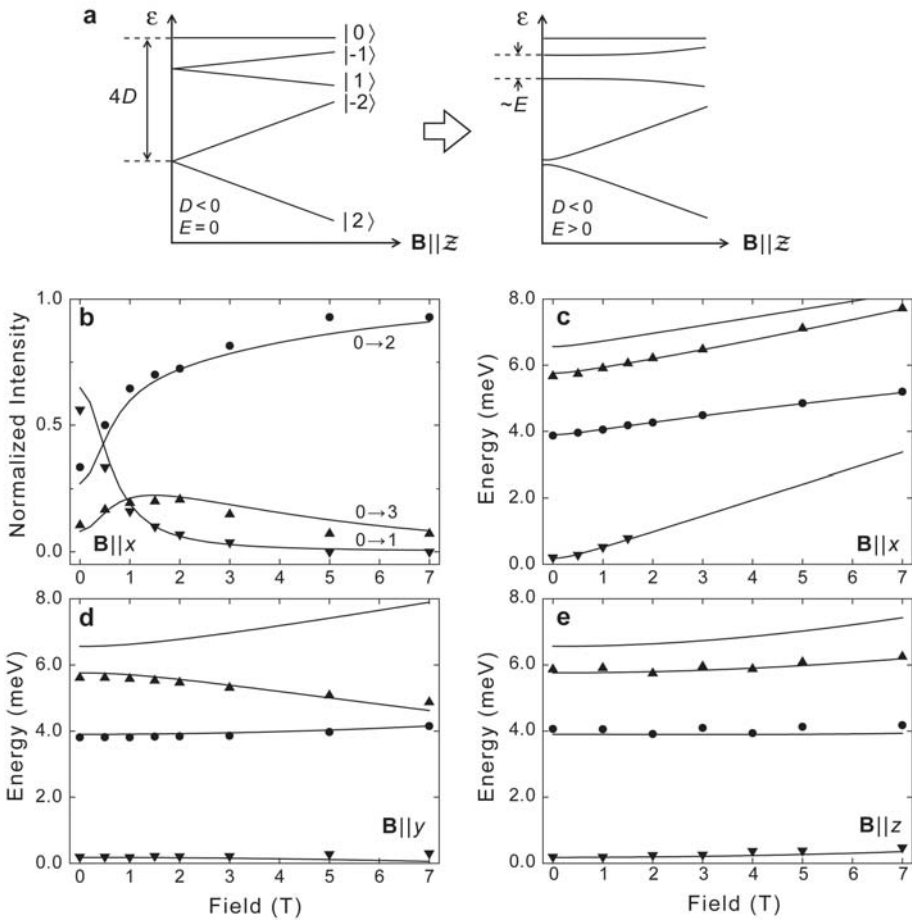

Figure 3.7: **(a)** Sketch of the qualitative effect of a finite E-value on an $S = 2$ system with negative D. **(b)** Step heights taken from fig. 3.6a. The solid lines show the calculated transition intensities based on (3.4). **(c–e)** Step positions acquired from fig. 3.6a–c, plotted together with the calculated excitation energies for Fe.

Thus $P_m(T)\Big(1 - P_n(T)\Big)$ quantifies the probability of simultaneously having a filled initial state $|\psi_m\rangle$ and an empty final state $|\psi_n\rangle$. The shape of the IETS transitions is given by:

$$\Phi(x) = \frac{1 + (x-1)\mathrm{e}^x}{\left(\mathrm{e}^x - 1\right)^2} \ . \tag{3.7}$$

This was derived for molecular vibration spectra [52, 53] and incorporates the thermal broadening caused by the finite temperature of the electrodes. To make sure that the summation runs only over positive energy excitations, the eigenstate indices n are assumed to be ordered with increasing energy ε_n. The

resulting modelled spectra for Fe (figs. 3.6d–f) correspond extremely well to the experimental data. Similar modelcurves for Mn are plotted together with the data in fig. 3.4.

The level of agreement between those modelled spectra and the experimental data is astonishing, considering that (apart from an overall scaling factor) no additional fitting is performed. For each type of atom the parameters S, g, D and E are determined once from the field dependence of the step energies and that information is sufficient to reconstruct a spectrum taken at any field strength or orientation.

3.4 Discussion

In this chapter we have presented a method to map the magnetic anisotropy of individual atoms using spin excitation spectroscopy. We find that Mn on Cu_2N has a weak easy-axis that is oriented out of plane with very little transverse contribution. Fe is shown to have an easy-axis along the N-row that has much higher anisotropy energy. Although the origin of these specific preferential directions remains to be explained, it is interesting to note that in either case it coincides with the directionality of the spin spreading calculated by DFT. The weakness of the anisotropy for Mn most likely results from the fact that a Mn atom has zero orbital angular momentum. Therefore the crystal field has no channel through which to influence the electronic spins.

For Fe we find $D = -1.55$ meV, corresponding to an energy barrier with height 6.2 meV. According to (3.1) this would result in a bit that is stable below ~ 2 K, if it were not for the significant transverse anisotropy $E = 0.31$ meV. Let us discuss the precise influence of this E-term on the magnetic stability. As shown in table 3.1, at zero field the two lowest-energy eigenstates are (almost) $\frac{1}{\sqrt{2}}\Big(|{-2}\rangle \pm |{+2}\rangle\Big)$. Regardless of whether the bit is set to '0' or to '1', one will measure $m = -2$ for 50% of the time and $m = +2$ for the other 50% of the time, making the system unsuitable for data storage. If, however, we were to apply a magnetic field of 2 T permanently over the bit in the $\mathcal{Z}$-direction, the two lowest states become:

$$|\psi_0\rangle = 0.99\,|{+2}\rangle - 0.12\,|{+0}\rangle + 0.09\,|{-2}\rangle, \text{ and}$$
$$|\psi_1\rangle = 0.10\,|{+2}\rangle + 0.12\,|{+0}\rangle - 0.99\,|{-2}\rangle.$$

These are stationary states that are still separated by a 6.0 meV barrier (i.e. stable at $T \lesssim 2$ K), but now one would measure $m = +2$ for 98% of the time if the bit is set to '0', and $m = -2$ for 98% of the time if set to '1'. This way Fe on Cu_2N can be considered a candidate for future laboratory demonstrations of an atomic bistable (albeit metastable in one of the two states) magnetic bit at low temperature.

Throughout the analysis we have used the free-atom spin values, $\frac{5}{2}$ for Mn and 2 for Fe, even though these are not at all necessarily correct for bound atoms. The DFT calculations presented in section 3.2 indicate that part of the

spin density spreads along the surface and into the bulk, suggesting a decrease in the effective spin on the atom. However, as a result of the discrete nature of the system, we can only adjust the quantum number S in steps of $\frac{1}{2}$ while the spin spreading is rather small.

Previously, for the case of Mn on Cu_2N, $S = \frac{5}{2}$ was found to explain the observed excitations better than any of the adjacent values [19]. For Fe, we use the following reasoning. Since we can clearly discern three excitations in the zero-field spectrum there should be at least four energy levels, ruling out any $S < \frac{3}{2}$. As will be derived in the next chapter, for any half-integer spin the zero-field degeneracy between states with equal $|m|$ cannot be broken by an E-term (Kramers degeneracy). This way we can additionally rule out any half-integer $S < \frac{7}{2}$. The remaining spin values are integer $S \geq 2$ or half-integer $S \geq \frac{7}{2}$, but as $S = \frac{5}{2}$ is the highest spin a d-shell magnet can adopt $S = 2$ is the only possibility left[3].

A point that remains unclear is the role of the orbital angular momentum of the electrons in the d-shell. Both the values for S and for g that we find (in each case close to $g = 2.00$ as expected for a pure electron spin) suggest that the orbital moment makes no substantial contribution to the effective spin vector $\hat{\mathbf{S}}$. One possibility is that the crystal field either quenches the orbital angular momentum or suppresses the spin-orbit coupling. However, this would in turn make the electron spins invulnerable to the influence of the crystal field which is clearly not the case.

The matrix elements (3.4) that were found to accurately determine the transition intensities are identical to those used for explaining inelastic neutron scattering in a magnetic molecular cluster (Fe_8) [51]. This could indicate that the observed inelastic tunneling arises from similar dipolar magnetic interactions between the spin of the tunneling electron and that of the magnetic atom. Especially for Fe the intensity of this process is remarkably large: at $B = 0$, the combined inelastic conductance (i.e. the sum of the IETS step heights) is larger than the elastic conductance (as measured at $V = 0$). Even the step of one of the individual transitions ($|\psi_0\rangle \rightarrow |\psi_1\rangle$) is at least as high as the background. This is surprising: not only does the excitation open a new inelastic conduction channel, its transmission is possibly even enhanced compared to the elastic path. A more detailed study of the inelastic excitations in comparison to the elastic current may provide insight into which electronic orbitals are involved in either process. In chapter 5 we will discuss a possible first step in that direction.

[3] In principle the interaction with the surface might destroy the d-shell character enough as to enable $S \geq 3$ (although the DFT calculations indicate a decrease of spin). This, however, does not fit our data as well as $S = 2$ does.